Dalton Transactions

ROYAL SOCIETY OF CHEMISTRY

PAPER

View Article Online
View Journal | View Issue

Cite this: *Dalton Trans.*, 2026, **55**, 854

Self-assembly of lanthanide-based single-ion magnets (SIMs) into 1D networks *via* Re(IV)-based metalloligands

Carolina Ferrari-Argachá,†[a] Santiago Valiero, †[a] Carlos Rojas-Dotti,[a] Aparicio Loaces,[a] Raúl Chiozzone, [a] Nicolás Moliner,[b] Leopoldo Suescun,[c] Joan Cano, [b] Francesc Lloret,[b] José Martínez-Lillo *[b] and Ricardo González*[a]

Received 7th August 2025,
Accepted 30th November 2025

DOI: 10.1039/d5dt01890k

rsc.li/dalton

Within the research field of molecular magnetism, single-ion magnets (SIMs) are of particular interest due to their ability to retain magnetic memory at the molecular level. At the same time, one-dimensional coordination polymers enable controlled spatial arrangement of magnetic centers, making them valuable models for investigating magneto-structural correlations. Here, we report the synthesis, crystal structure, magnetic properties and theoretical calculations of a family of five one-dimensional Re(IV)–Ln(III) coordination complexes obtained by using the "complex-as-ligand" strategy and based on the pyridinedicarboxylic acid derivatives that form the $[ReBr_5(3,4\text{-}pydcH_2)]^-$ and $[ReBr_5(3,5\text{-}pydcH_2)]^-$ metalloligands, with general formulas $(NBu_4)_2\{Ln(EtOH)(dpkOEt)[ReBr_5(3,5\text{-}Hpydc)]_2\}_n \cdot 3.5H_2O \cdot MeOH$ [Ln = Dy(**2**), Tb(**3**)] and $\{Ln[ReBr_5(3,4\text{-}pydc)](dmf)_3(MeOH)\}_n \cdot dmf$ [Ln = Dy(**4**), Tb(**5**), Gd(**6**)]. Two of these Re(IV)–Ln(III) compounds—$[Dy(EtOH)(dpkOEt)\{ReBr_5(3,5\text{-}Hpydc)\}_2]_n$ (**2**) and $[Dy\{ReBr_5(3,4\text{-}pydc)\}(dmf)_3(MeOH)]_n$ (**4**)—exhibit slow relaxation of the magnetisation, which is characteristic of SIM behaviour and accounted for ac magnetic susceptibility measurements. Structural analyses suggest that intra- and intermolecular halogen–halogen (Br···Br) interactions may influence the magneto-structural properties of **2–6**. These findings demonstrate the potential of Re(IV)–Ln(III) hybrid systems as candidates for developing magnetically addressable molecular materials.

Introduction

In recent decades, molecular magnetic materials have garnered considerable attention due to their promising applications in various research fields and advanced technologies, including high-density storage systems, qubits for quantum computing, and molecular spintronics and electronics.[1–7] Within the molecular magnetism research field, discrete complexes exhibiting slow magnetic relaxation phenomena, commonly referred to as Single-Molecule Magnets (SMMs), Single-Ion Magnets (SIMs) and one-dimensional coordination polymers known as Single-Chain Magnets (SCMs), have emerged as particularly well-studied materials.[8–15] Notably, a middle-step type of material occupies a conceptual space between SMMs/SIMs and SCMs: chains of SMMs/SIMs. These structures are also coordination polymers, in which the spin carriers are interconnected by organic ligands to form one-dimensional arrangements. However, in contrast to SCMs, these chains present no magnetic exchange between the spin carriers. This phenomenon is primarily facilitated by the incorporation of large ligands and the use of lanthanide metal ions, whose particularly penetrating 4f orbitals make them a more restrained type of metal ion in terms of magnetic exchange. This unique structural and electronic configuration allows for the retention of the individual magnetic properties of SMMs or SIMs within a one-dimensional motif.[16,17]

Most of the compounds that exhibit these attracting magnetic behaviours are homo- and heteronuclear complexes based on 3d or 4f metal ions. The design, synthesis and magnetostructural characterisation of this type of material are key steps for the comprehension of the unusual quantum physics related to their properties. Research carried out on these systems reveals that large magnetic anisotropies and total spin values of the molecules (S) may favour and enhance the slow magnetic relaxation phenomenon. In the light of this knowledge, 4d and 5d metal ions are excellent candidates as starting materials for the development of new homo- and heteropolynuclear magnetic complexes, given their high values of spin–

[a]*Área Química Inorgánica, Departamento Estrella Campos, Facultad de Química, Universidad de la República, General Flores 2124, Montevideo, Uruguay. E-mail: rgonzale@fq.edu.uy*
[b]*Departament de Química Inorgánica/Instituto de Ciencia Molecular (ICMol), University of Valencia, c/Catedrático José Beltrán 2, Paterna, Valencia 46980, Spain. E-mail: f.jose.martinez@uv.es*
[c]*Cryssmat-Lab/DETEMA, Facultad de Química, Universidad de la República, General Flores 2124, Montevideo, Uruguay*
†These authors contribute equally to this work.

orbit coupling constant (λ) and high S values of the ground state.[18] In fact, combining lanthanides with 4d or 5d metal ions would be a substantial step in the crystal engineering process to obtain new heteropolynuclear compounds with large magnetic anisotropy.[19,20]

In this regard, Re^{IV} is an excellent candidate, being a 5d metal ion with a λ value of *ca.* 1000 cm^{-1} and a d^3 electronic configuration with three unpaired electrons in its typical distorted octahedral environment. These features account for the high magnetic anisotropy of the S = 3/2 ground state.[21,22] Besides, the diffuseness of its magnetic orbitals gives rise to large spin delocalisation towards the ligands, favouring slow relaxation of the magnetisation phenomenon.[22,23] Proof of this are the several Re^{IV}-based SMMs and SCMs reported in the literature to date, some of which exhibit remarkable magnetic behaviour among 5d-based systems. Nonetheless, there exist only two reported studies on the magnetic properties of Re^{IV}–Ln^{III} systems.[19,20]

In this context, we have focused our research work on one-dimensional Re^{IV}–Ln^{III}-based compounds (Ln^{III} being a lanthanide metal ion). For this, we have used the strategy of "complex-as-ligand".[22] Thus, 3,4-pyridinedicarboxylic acid (3,4-H_2pydc) and 3,5-pyridinedicarboxylic acid (3,5-H_2pydc) have been used as organic "pre-ligands" (Scheme 1). They coordinate first to the Re^{IV} ions through the nitrogen atoms and the carboxylate groups remain free for coordinating to the lanthanide ions. Moreover, with the aim of blocking coordination positions, di(2-pyridyl) ketone (dpk) has also been used.[24] However, in the presence of a metal ion dissolved in an alcoholic solution (ethanol in our case), this ligand reacts with the solvent and the formation of the hemiacetal derivative (dpkOEt) takes place; the resulting two molecules are shown in Scheme 2.

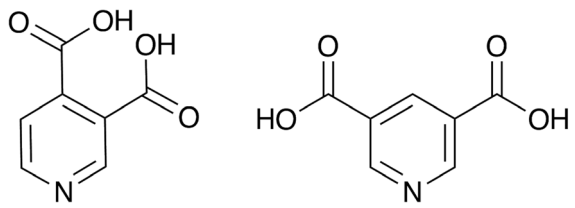

Scheme 1 Molecular structure of the 3,4-H_2pydc (left) and 3,5-H_2pydc (right) ligands.

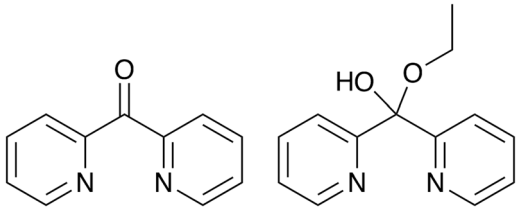

Scheme 2 Molecular structure of the dpk (left) and HdpkOEt (right) ligands.

Hence, we report the synthesis and structural, theoretical and magnetic characterisation of a new Re^{IV} complex with the formula $(NBu_4)_3[ReBr_5(3,4\text{-pydcH}_2)][ReBr_5(3,4\text{-pydcH})]\cdot H_2O$ (**1**), and five new Re^{IV}–Ln^{III} heteropolynuclear complexes, two of which have the formula $(NBu_4)_2\{Ln(EtOH)(dpkOEt)[ReBr_5(3,5\text{-Hpydc})]_2\}_n\cdot 3.5H_2O\cdot MeOH$ [Ln = Dy(**2**), Tb(**3**)] and the last three present the general formula $\{Ln[ReBr_5(3,4\text{-pydc})](dmf)_3(MeOH)\}_n\cdot dmf$ [Ln = Dy(**4**), Tb(**5**), Gd(**6**)]. From this family of complexes, **2** and **4** exhibit a field-induced slow relaxation of the magnetisation phenomenon.

Experimental

Materials and physical measurements

All reagents were of commercial origin and were used as received. All manipulations were performed under aerobic conditions. The Re^{IV} precursor K_2ReBr_6 was prepared following the synthetic method described in the literature.[25] Elemental analyses (C, H, N) were performed in an elemental analyzer (CE Instruments CHNS1100) and the molar ratio between heavier elements was found by means of a Philips XL30 scanning electron microscope (SEM/EDAX), equipped with an X-ray microanalysis system, at the Central Service for the Support to Experimental Research (SCSIE) at the University of Valencia. Infrared (IR) spectra of **1** and **6** were recorded with a PerkinElmer Spectrum 65 FT-IR spectrometer in the 4000–400 cm^{-1} region. Variable-temperature, solid-state (dc and ac) magnetic susceptibility data were collected on a Quantum Design MPMS-XL SQUID magnetometer equipped with a 5 T dc magnet. Experimental magnetic data were corrected for the diamagnetic contributions of both the sample holder and eicosane. The diamagnetic contribution of the individual atoms was corrected by using Pascal's constants.[26]

X-ray diffraction data of compounds **1** and **4–6** were collected on a Bruker D8 Venture diffractometer with a PHOTON II detector by using monochromatised Mo-K_α radiation (λ = 0.71073 Å), while data on single crystals of **2** and **3** were collected on a Rigaku Oxford Diffraction SuperNova diffractometer with graphite-monochromated Mo-K_α radiation (λ = 0.71073 Å). Crystal parameters and refinement results for **1–6** are summarised in Table S1. The crystal structures were solved by an intrinsic phasing structure solution method using ShelXT and subsequently completed by Fourier recycling using the SHELXL-2018/3 software packages and refined by the full-matrix least-squares refinements based on F^2 with all observed reflections.[27] Larger-than-expected residuals are observed for **1–3** and **6**, which suggests slight unresolved disorder or twinning. As discussed below, this structural noise can be understood in light of the considerable amount of crystallization solvent present in the mentioned structures and the thermal disorder of the tetrabutylammonium cation molecules. Even so, the molecular assignments are unambiguous in every case, and all the molecules are perfectly consistent from the chemical standpoint. CCDC 2407414 (**1**), 2407412 (**2**), 2407411 (**3**), 2407413 (**4**), 2407409 (**5**) and 2407410 (**6**).

Preparation

Synthesis of $(NBu_4)_3[ReBr_5(3,4\text{-pydcH}_2)][ReBr_5(3,4\text{-pydcH})]\cdot H_2O$ (1). To synthesise compound **1**, 0.1 mmol of the rhenium precursor $(NBu_4)_2[ReBr_6]$ (115 mg) and 0.667 mmol of the ligand (3,4-H_2pydc) (111.4 mg) were dissolved in 10 mL of a 1 : 2 acetone/isopropanol mixture. The mixture was heated to reflux for 3 hours, resulting in an intense orange solution. The solution was filtered and allowed to evaporate slowly at room temperature. After approximately one week, orange crystals in the form of thin plates suitable for X-ray diffraction were obtained. Yield 60%. Selected IR data [KBr, ν_{max}/cm^{-1}] are as follows: 2961vs, 2931s, 2874s, 1734vs, 1481s, 1375s, 1265m, 1150w, 1063m, 1036w, 810vw, 741vw, 632vw. Elemental analysis calculated (found) for $C_{62}H_{119}Br_{10}N_5O_9Re_2$ (**1**): C, 33.1 (33.2); H, 5.3 (5.3); N, 3.1 (3.2)%.

Synthesis of $(NBu_4)_2\{Ln(EtOH)(dpkOEt)[ReBr_5(3,5\text{-Hpydc})]_2\}_n\cdot 3.5H_2O\cdot MeOH$; Ln = Dy(2), Tb(3). **2** and **3** were synthesised by dissolving the corresponding $LnCl_3\cdot 6H_2O$ salt (*ca.* 11.3 mg, 0.03 mmol) and dpk (5.5 mg, 0.03 mmol) in ethanol (3 mL). The reaction mixture was stirred for 15 minutes. Then, $NBu_4[ReBr_5(3,5\text{-H}_2\text{pydc})]$ (30 mg, 0.03 mmol) dissolved in methanol (3 mL) was added. The final mixture was stirred for another 15 minutes and filtered. After 5 days of slow evaporation of the solvent, orange crystals suitable for X-ray diffraction were obtained. The obtained crystals were stored at room temperature under aerobic conditions for further analyses (see the SI). Yield 35%. Selected IR data [KBr, ν_{max}/cm^{-1}] are as follows: 2961vs, 2873s, 1618vs, 1569s, 1458s, 1383s, 1155w, 1125m, 879w, 770w, 734w, 632vw, and 518vw. Elemental analysis calculated (found) for $C_{61}H_{86}N_6O_{17}Br_{10}Re_2Dy$ (**2**): C 29.2 (29.0); H 3.5 (3.4); N 3.4 (3.3)% and $C_{61}H_{86}N_6O_{17}Br_{10}Re_2Tb$ (**3**): C 29.2 (29.1); H 3.5 (3.2); N 3.4 (3.4)%.

Synthesis of $\{Ln[ReBr_5(3,4\text{-pydc})](dmf)_3(MeOH)\}_n\cdot dmf$; Ln = Dy(4), Tb(5), Gd(6). Compounds **4–6** were synthesised by dissolving the corresponding $LnCl_3\cdot 6H_2O$ salt (*ca.* 5.0 mg, 0.01 mmol) and dpk (5.5 mg, 0.03 mmol) in a mixture of ethanol/methanol (2 : 1, 3 mL). Immediately, 1 mL of dmf was added. After stirring for 10 minutes, a solution of **1** dissolved in 1.5 mL of methanol was added. At this point, precipitation was observed and one more mL of dmf was added, which resulted in a clear orange solution. The mixture was stirred at room temperature for 30 minutes and stored in a closed beaker. The formation of orange crystals, which were suitable for single-crystal X-ray diffraction studies, was observed after 6 days. Yield *ca.* 60%. Elemental analysis calculated (found) for $C_{20}H_{35}N_5O_9Br_5ReDy$ (**4**): C, 19.5 (19.4); H, 2.9 (2.9); N, 5.7 (5.7)%; for $C_{20}H_{35}N_5O_9Br_5ReTb$ (**5**): C, 19.5 (19.5); H, 2.7 (2.7); N, 5.7 (5.7)%; and for $C_{20}H_{35}N_5O_9Br_5ReGd$ (**6**): C, 19.5 (19.1); H, 2.7 (2.7); N, 5.7 (5.4)%.

Theoretical calculations

All calculations were performed in the ORCA software suite version 6.0,[28] by using cropped models from the experimental crystal structure as input (see the SI). Magnetic coupling constants were evaluated by DFT calculations *via* the *broken symmetry* (BS-DFT) formalism using the B3LYP hybrid functional and the geometry of a dimer consisting of the two closest anionic units of **1** (Fig. S4) and cropped models 1–3 of **6** (Fig. S5). The def2-svp basis set was used for all atoms but Re and Gd, for which the segmented all-electron relativistically contracted (SARC)-tzvp basis set was used.[29] The evaluation of Coulomb and exchange two-electron integrals was accelerated using the resolution of identity (RI) and the chains of spheres (COSX) approximations with an automatically generated auxiliary basis set. In all cases, a very tight energy convergence threshold ($\Delta E < 1.0 \times 10^{-9}$ au) was adopted. Wavefunction stability was verified at each step through ORCA's stability test to ensure convergence to the most stable electronic configuration.

To estimate the Landé *g* factor and the components of the Zero-Field Splitting (ZFS), Complete Active Space Self-Consistent Field (CASSCF) calculations were performed on both the diprotonated molecular unit of **1** and cropped model 1 (CM1), complemented by N-electron valence-state perturbation theory (CASSCF/NEVPT2) to account for correlation effects.[30] An active space composed of 3 electrons and 5d-orbitals with 10 roots for quartet states and 20 for doublet states was selected for calculations in both cases. For CASSCF calculations on CM1, the diamagnetic ion substitution technique was used, for which both Gd(III) ions were replaced with diamagnetic Lu(III) ions, thus simplifying the electronic configuration of the system.

Results and discussion

Synthesis and characterisation

By using the anionic mononuclear complexes $[ReBr_5(3,5\text{-pydcH}_2)]^-$ and $[ReBr_5(3,4\text{-pydcH}_2)]^-$ as rhenium(IV)-based building blocks, five novel one-dimensional complexes have been obtained. In pursuit of this goal, compound **1** was synthesised following a synthetic methodology similar to that previously described for $NBu_4[ReBr_5(3,5\text{-pydcH}_2)]$.[20]

Thus, by reacting $NBu_4[ReBr_5(3,5\text{-pydcH}_2)]$ with a mixture of the corresponding Ln^{III} ion and dpk, compounds **2** and **3** are obtained. It is noteworthy to mention that the ligand coordinating the lanthanide ions is the hemiacetalic form of dpk (dpkOEt), prepared through the reaction between dpk and ethanol, which is catalysed by the presence of the metal ion.[24]

Under similar synthetic conditions but using the anionic complex of **1** as a metalloligand, insoluble powders are obtained. To avoid this problem, a couple of mL of dmf are added to obtain clear solutions. Since dmf is a highly coordinating solvent, it replaces the dpkOEt molecule in the coordination sphere of the lanthanides, and thus compounds **4–6** are obtained. Noteworthily, when dpk is omitted as a reagent, none of these compounds are obtained; this fact suggests that dpk is needed for the formation of intermediate reaction species.

Crystal structure

Compound of formula $(NBu_4)_3[ReBr_5(3,4\text{-pydcH}_2)][ReBr_5(3,4\text{-pydcH})]\cdot H_2O$ (1). Compound **1** crystallises in the

monoclinic system with space group $P2_1/c$ (Table S1). The crystal structure comprises negatively charged molecules of the mononuclear Re^{IV} complex, which are protonated and half-deprotonated, along with tetrabutylammonium cations (NBu_4^+), that maintain the charge balance, and water molecules of crystallisation. More specifically, the asymmetric unit is composed of one protonated and one half-protonated $[ReBr_5(3,4\text{-pydcH}_x)]^-$ (x = 1 and 2) anions, three NBu_4^+ cations and one water molecule of crystallisation (Fig. 1).

The Re^{IV} ions in **1** keep the distorted octahedral geometry similar to that previously reported for the analogous complex $NBu_4[ReBr_5(3,5\text{-pydcH}_2)]$.[20] The Re–Br bond lengths [average value of 2.487(1) Å] agree with those found in previously reported Re^{IV}–bromide complexes.[31–35] In the same way, C–C, C–N and C–O bond lengths are in the range of the expected ones for the 3,4-pydcH$_2$ ligand (Scheme 1) and counter ion molecules.

The structure is held together by electrostatic forces, halogen and hydrogen bonds and van der Waals interactions. Short intermolecular halogen contacts occur between adjacent anionic complexes, with Br···Br distances [*ca.* 3.82 Å], which generate intercalated dimeric units. These systems are connected along the *c* axis by further Br···Br interactions [*ca.* 4.26 Å], creating a one-dimensional motif. Along the same axis, carboxylate groups and crystallisation water molecules are H-bonded, with O···O distances ranging from 2.62 to 2.99 Å. Intramolecular hydrogen bonds within the half-protonated anionic $[ReBr_5(3,5\text{-pydcH})]^{2-}$ molecules are also found [O···O distances of *ca.* 2.39 Å]. Considering the intermolecular interactions, the mononuclear units of compound **1** form a supramolecular 2D structure. The space between each of these planes is filled by NBu_4^+ cations, which prevent direct contacts among the 2D anionic sheets (the third shortest Br···Br contact being *ca.* 5.38 Å).

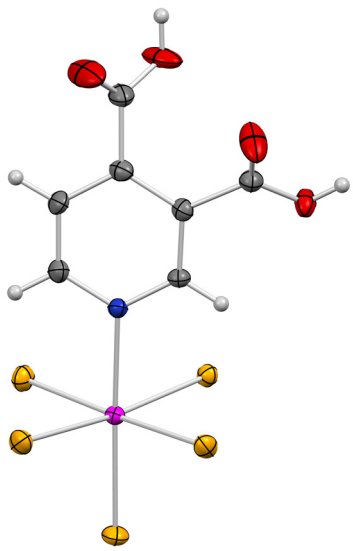

Fig. 1 Diprotonated mononuclear unit of compound **1**. Tetrabutylammonium cations and water molecules have been omitted for clarity. Colour code: Re, pink; Br, orange; O, red; N, blue; C, grey; and H, white.

Complexes of formula $(NBu_4)_2\{Ln(EtOH)(dpkOEt)[ReBr_5(3,5\text{-Hpydc})]_2\}\cdot 3.5H_2O\cdot MeOH$ (2 and 3)

2 and **3** are isostructural compounds that crystallise in the monoclinic system with the $P2_1/c$ space group (Table S1). Their crystal structures comprise negatively charged chains placed along the crystallographic *a* axis, which include Re^{IV} and Ln^{III} [Ln^{III} = Dy (**2**) and Tb (**3**)] ions interconnected through the 3,5-Hpydc ligand. The charge balance is guaranteed by the presence of NBu_4^+ cations. Solvent molecules of crystallisation are also present.

Within each structure, there are two Re^{IV} and one Ln^{III} crystallographically independent ions. The existence of two independent Re^{IV} ions accounts for the distinct coordination modes and different protonation degrees that carboxylate groups of the metalloligand exhibit. This phenomenon has already been reported for a different Re^{IV}–Dy^{III} system.[20] Thus, the anionic Re^{IV} complexes are arranged around the periphery of the central one-dimensional motif, serving as a structural backbone of the reported chains (Fig. 2).

The Re^{IV} ions in **2** and **3** maintain the distorted octahedral geometry of the metalloligand precursor. The lanthanide ions exhibit a coordination number of 9, showing a tricapped trigonal prismatic geometry (Fig. 2). In an alternative way to describe it, there is an equatorial plane forming a distorted pentagon with vertices occupied by oxygen atoms from four different molecules of the metalloligand. One of these exhibits a bidentate coordination mode, while the remaining three are of monodentate nature. The apical position of the prism is occupied by the oxygen atom of an EtOH molecule, whereas the triangular base is completed by two nitrogen and one oxygen atoms belonging to the tridentate $(dpkOEt)^-$ ligand. The average $Ln–O_{carboxylate}$ distances are 2.402 (**2**) and 2.416 (**3**) Å, while the $Ln–O_{EtOH}$ distance falls within the 2.36(1)–2.41(1) Å range.

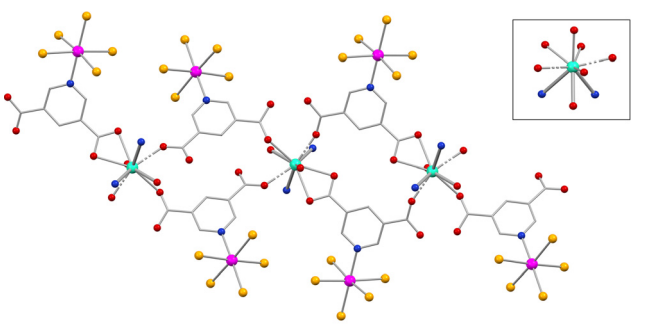

Fig. 2 View of the 1D motif of compounds **2** and **3** generated by lanthanide(III) ions [Ln^{III} = Dy (**2**) and Tb (**3**)] linked by the rhenium(IV)-based metalloligands. H atoms, NBu_4^+ cations, dpkOEt molecules and solvent crystallisation molecules are omitted for clarity. The inset shows the coordination sphere of the lanthanide ion. Colour code: Re, magenta; Br, brown; O, red; N, blue; C, grey; and Ln, turquoise.

A careful analysis of the C–O bond lengths within the carboxylate groups of the metalloligands confirms that one of these groups remains protonated. In these cases, the coordination of the lanthanide ions occurs through the carbonyl group (C=O). Conversely, only the bidentate-coordinating carboxylate unit is fully deprotonated. Furthermore, these protonated carboxylate groups form two types of intramolecular hydrogen bonds. One occurs between oxygen atoms O(4) and O(8), belonging to adjacent carboxylate groups, with an O···O distance of approximately 2.40(1) Å. The second one is formed between the protonated carboxylate group [O(6)] and the oxygen atom from the coordinated $(dpkOEt)^-$ ligand [O(9)], with an O···O distance of approximately 2.51(1) Å.

Each compound exhibits two different intramolecular Ln···Ln distances of 8.64(1) and 10.08(1) Å and, similarly, two different Re···Ln separations of approximately 7.95(1) and 8.52(1) Å. Bulky NBu_4^+ cations ensure that adjacent chains remain structurally isolated. The shortest Re–Br···Br–Re distance between two adjacent chains is *ca.* 4.36(1) Å, which is larger than the sum of the van der Waals radii of bromide anions [*ca.* 3.90(1) Å]. This representation shows that there is no direct interaction between the anionic chains and that the bulky NBu_4^+ cations are responsible for these structural features. Additionally, intramolecular Re–Br···Br–Re interactions are observed (Fig. 3). These interactions involve the Re(1) and Re(2) subunits, which interact through Br(1) and Br(9) at a distance of 3.55(1) Å. This type of intramolecular interaction is important from a magnetostructural viewpoint.

These crystal structures of **2** and **3** are held together by electrostatic forces and van der Waals interactions. Hydrogen bonds based on water, methanol and/or ethanol molecules of crystallisation are likely to be present. However, these cannot be determined due to the high degree of disorder of the crystallization solvent.

Positional disorder has also been observed in the carbon atoms of the NBu_4^+ molecules. These local disorders have been modelled by using appropriate restraints and constraints.

Complexes of formula $\{Ln[ReBr_5(3,4\text{-pydc})](dmf)_3(MeOH)\}_n\cdot dmf$ (4–6). Compounds **4–6** are isostructural and crystallise in the triclinic system with the $P\bar{1}$ space group (Table S1). The molecular structure of these complexes consists of a mixed neutral chain based on Re^{IV} and Ln^{III} [Ln^{III} = Dy (**4**), Tb (**5**) and Gd (**6**)] ions and dmf as the crystallisation solvent. Lanthanides and rhenium centers are bridged through the $(3,4\text{-pydc})^{2-}$ ligand and, additionally, each Ln^{III} ion is also coordinated by one MeOH and three dmf molecules. The coordination environment at the rhenium^{IV} ion is maintained from the metalloligand precursor. Moreover, there is one dmf crystallization molecule per asymmetric unit.

In all these crystal structures, there is only one Re^{IV} and one Ln^{III} ions which are crystallographically independent. In contrast to **2** and **3**, in compounds **4–6**, the Re^{IV}-based building block is fully deprotonated, featuring the $[ReBr_5(3,4\text{-pydc})]^{3-}$ unit. Thus, the negative charges of the Re^{IV} precursor compensate for the charge of the trivalent lanthanide, leading to the formation of neutral chains (Fig. 4).

Hence, the 1D motif found in **4–6** consists of a chain of Ln^{III} cations placed in two alternating positions along the *a* axis. The chains are linked together by the $[ReBr_5(3,4\text{-pydc})]^{3-}$ unit, which is placed peripherally to the central Ln^{III} ions, generating a one-dimensional motif (Fig. 4).

Two different $Ln^{III}\cdots Ln^{III}$ distances are present in each structure. The shortest distance in **4–6** ranges from 5.23(1) to 5.26(1) Å, whereas the largest distance is between 5.74(1) and 5.76(1) Å.

In **4–6**, the octacoordinate Ln^{III} ions exhibit a distorted squared antiprism geometry, where all the coordinating atoms are oxygen (Fig. 4). Three of these oxygen atoms correspond to coordinating dmf molecules [O(1A), O(1B), and O(1C)] and one comes from a coordinating methanol molecule [O(1E)]. The four remaining oxygen atoms [O(1)–O(4)] belong to three

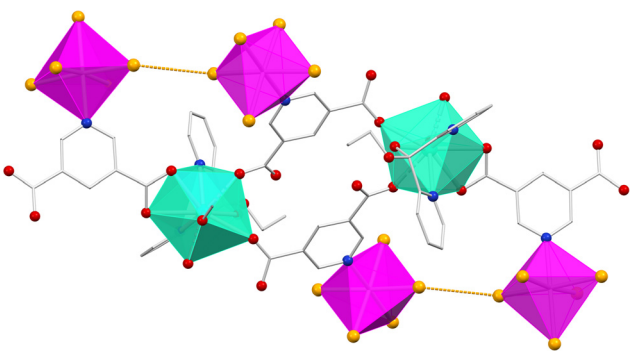

Fig. 3 Intramolecular Br···Br interactions (solid orange line) in **2** and **3**. H atoms, NBu_4^+ cations and solvent crystallisation molecules are omitted for clarity. Colour code: Re, magenta; Ln, turquoise; Br, brown; O, red; N, blue; and C, grey.

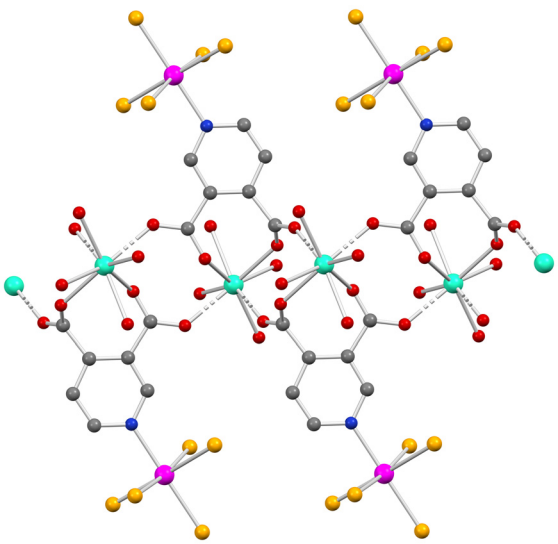

Fig. 4 View of the 1D motif of compounds **4–6** made up of the lanthanide(III) ions [Ln^{III} = Dy (**4**), Tb (**5**) and Gd (**6**)] linked by the rhenium(IV)-based metalloligands. H atoms and dmf molecules are omitted for clarity. Colour code: Re, pink; Ln, turquoise; Br, brown; O, red; N, blue; and C, grey.

different $[ReBr_5(3,4\text{-pydc})]^{3-}$ units. Thus, one of them acts as a chelating ligand forming a 7-member ring, whereas the two remaining metalloligand molecules form the bridging Ln···Ln···Ln linear motif.

In all cases, the anionic $[ReBr_5(3,4\text{-pydc})]^{3-}$ units present a tetramonodentate coordination mode, where the oxygen atoms [O(2) and O(3)] are involved in the chelate formation, while the outer oxygen atoms [O(1) and O(4)] are those coordinating the second and third lanthanide ions, respectively.

It must be noted that, in compounds **4–6**, one of the dmf molecules, namely dmf(C), presents a slight positional disorder distributed in two most probable positions. Due to this disorder, the corresponding [O1C]···Ln^{III} bond length varies by *ca.* 0.07 Å.

As shown in Fig. 4, the molecular chains extend along the crystallographic *a* axis. Among four neighbouring chains, an empty cavity appears, which is occupied by dmf crystallisation molecules. In fact, the existence of these solvent crystallisation molecules seems to produce enough steric hindrance to keep the chains relatively isolated. Thus, the two shortest Br···Br interchain distances are *ca.* 4.43(1) and 5.87(1) Å. As mentioned above, this fact is of strong relevance in what the magnetic properties of the systems concern and will be thoroughly discussed in the next section.

Because of the neutral nature of the complexes in **4–6**, the whole structure is linked together by weak van der Waals interactions. Furthermore, hydrogen bonding interactions between the dmf crystallisation molecule [O(1E)] and the coordinated MeOH molecule [O(1D)] [the average O(1E)···O(1D) separation is approximately 2.80(1) Å] contribute to stabilising their crystal packing.

Magnetic properties

Dc magnetic susceptibility. The magnetic properties of the reported compounds were studied through direct current (dc) magnetic susceptibility measurements. The studies were carried out on microcrystalline samples of **1–6** in the temperature range of 2–300 K under an external dc field of 0.5 T. The six complexes present a similar behaviour that is represented in the form of a $\chi_M T$ *versus* T plot in Fig. 5 and Fig. S1 (χ_M being the molar magnetic susceptibility per two Re^{IV} units in **1**, per $Re^{IV}{}_2Ln^{III}$ unit in **2** and **3**, per $Re^{IV}Ln^{III}$ unit in **4** and **5** and per two $Re^{IV}Ln^{III}$ units in **6**). At room temperature, $\chi_M T$ values are 3.35 (**1**), 17.91 (**2**), 14.67 (**3**), 15.68 (**4**), 14.31 (**5**) and 18.97 $cm^3\ mol^{-1}\ K$ (**6**). These experimental data are in agreement with the expected ones for the magnetically isolated spin carriers in the abovementioned units, considering that Re^{IV} ion presents $S_{Re} = 3/2$ and $g \approx 1.9$, Dy^{III} ion has a fundamental term $^6H_{15/2}$, $J_{Dy} = 15/2$ and $\chi_M T \approx 14.17\ cm^3\ mol^{-1}\ K$, Tb^{III} ion has a fundamental term $^7F_6$, $J_{Tb} = 6$ and $\chi_M T \approx 11.82\ cm^3\ mol^{-1}\ K$ and Gd^{III} ion has a fundamental term $^8S_{7/2}$, $J_{Gd} = 7/2$ and $\chi_M T \approx 7.88\ cm^3\ mol^{-1}\ K$.

With decreasing temperature, $\chi_M T$ values remain approximately constant following Curie's law behaviour up to 100 K for all compounds except **4**, which presents a decrease of $\chi_M T$ values from 150 K. At lower temperatures, the decrease of $\chi_M T$ values is observed in all the complexes reaching figures of 1.48 (**1**), 11.57 (**2**), 8.10 (**3**), 9.40 (**4**), 7.86 (**5**) and 17.04 $cm^3\ mol^{-1}\ K$ (**6**).

This phenomenon occurs mostly because of the depopulation of the high energy levels of the lanthanide and rhenium ions and their intrinsic magnetic anisotropy. It must be pointed out that the values observed at 2.0 K in **1–6** are lower than the ones expected for the sum of the isolated spin carriers. This can be explained by the existence of short Re–Br···Br–Re contacts in their crystal structures. In the case of **1**, these contacts result in significant intermolecular interactions as usually observed for this type of mononuclear Re^{IV}–bromide-based compounds.[33] **2** and **3** present significant intramolecular interactions, as described above (see the Crystal structure section), which are not observed in **4–6**. These last three complexes still present long intermolecular Br···Br contacts, which may explain the observed phenomena. The magnetic interactions involving lanthanide ions are in

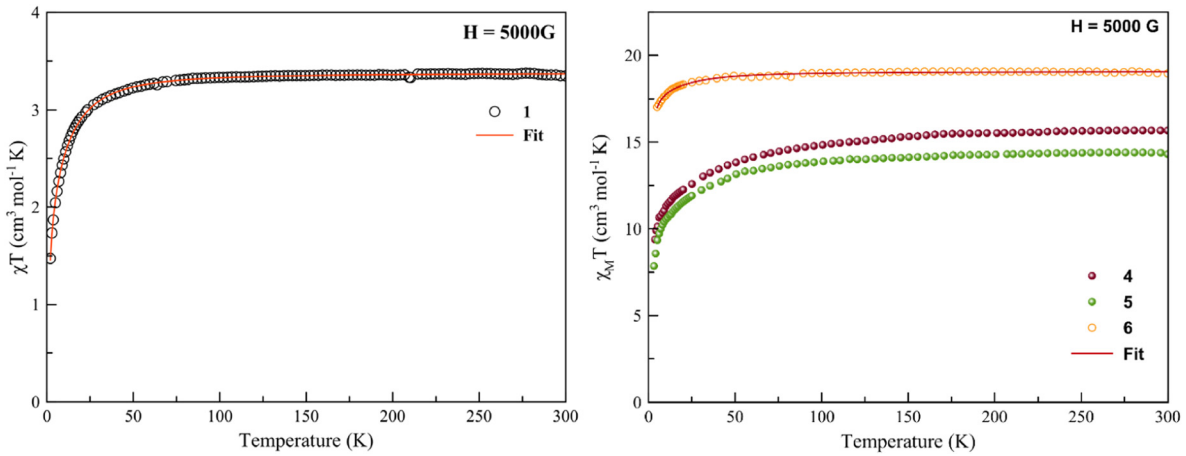

Fig. 5 Thermal variation of the $\chi_M T$ product per two Re^{IV} units for **1** (left) and per one $Re^{IV}Ln^{III}$ unit for **4** and **5** and two $Re^{IV}Ln^{III}$ units for **6** (right). The solid red line represents the best theoretical fit of the experimental data. Best-fit parameters are summarized in Table 1.

general quite small due to the internal distribution of f electrons. In this sense, no appreciable magnetic interactions between the lanthanide ions in **2–6**, connected through extended OC–(CCC)–CO and OCO pathways, should be expected.[20,36]

Through the appropriate phenomenological spin Hamiltonian, the experimental data of compounds **1** and **6** have been fitted. Firstly, for the mononuclear compound **1**, the Zero-Field Splitting (ZFS) of the Re^{IV} ion and the Zeeman effect and the magnetic exchange are considered as described in eqn (1):

$$\begin{aligned}\hat{H} = {} & D[(\hat{S}_{zRe1})^2 + (\hat{S}_{zRe2})^2 - 5/2] + g_{\parallel}\beta H_z(\hat{S}_{zRe1} + \hat{S}_{zRe2}) \\ & + g_{\perp}\beta(H_x\hat{S}_{xRe1} + H_y\hat{S}_{yRe1} + H_x\hat{S}_{xRe2} + H_y\hat{S}_{yRe2}) \\ & - 2J(\hat{S}_{Re1}\cdot\hat{S}_{Re2}).\end{aligned} \quad (1)$$

Herein, $\hat{S}_x$, $\hat{S}_y$ and $\hat{S}_z$ are the spin operators, H_x, H_y, and H_z are the components of the magnetic field along the coordinate axes x, y and z, $g_{\parallel}$ and $g_{\perp}$ are the parallel and perpendicular components of the g tensor, respectively, μ_B is the Bohr magneton and D is the energy gap between the ±3/2 and ±1/2 Kramers doublets, or ZFS, in the absence of an external magnetic field. This model considers that adjacent anions interact through the magnetically relevant short intermolecular Br···Br contacts as well (Fig. S4). Regarding this model, the magnetic exchange term is included, with J being the magnetic exchange constant.[20]

The parameters obtained for the best fit from least-squares calculations are $|D|$ = 7.39(4) cm^{-1}, g = 1.89(1) and J = −0.22(1) K with R = 99.1% ($g = g_{\perp} = g_{\parallel}$ was assumed in order to avoid over-parameterisation; R is the residual factor defined as $\left[\sum_i^{\text{points}} (M_{exp} - M_{calc})^2\right]\left[\sum_i^{\text{points}} (\chi_{exp} - M\chi_{calc})^2\right]$).[37]

As shown in Fig. 6, the calculated curve for **1** reproduces very well the magnetic data in the whole temperature range. Similar $|D|$ and J values have been found in the literature for analogous mononuclear compounds of the type $NBu_4[ReX_5L]$ with X = Cl or Br.[20,38,39]

Theoretical NEVPT2 studies on the anionic $[ReBr_5(3,4\text{-pydcH}_2)]^-$ unit were performed to compare the previous results from the least-squares calculations with those obtained theoretically. Thus, the NEVPT2 computed results are $|D|$ = 7.08(1) cm^{-1}, g_{Re} = 1.79(1) and E/D = 0.31(1). A similar value for the E/D ratio was obtained previously for the $(PPh_4)_2[trans\text{-}ReF_4(CN)_2]$ complex through HFEPR experiments.[40] Due to the E/D coefficient being close to 1/3, extracting the sign of D becomes questionable, as at the high rhombicity limit, the energy levels become symmetric with respect to the transformation $D \rightarrow -D$, and thus the sign of D has no effect on the values of Dx, Dy and Dz.

Furthermore, BS-DFT calculations performed on a dinuclear model containing the closest two $[ReBr_5(3,4\text{-pydcH}_2)]^-$ and $[ReBr_5(3,4\text{-pydcH})]^{2-}$ units in the crystal structure (Fig. S4, d = 3.82 Å) showed a theoretical antiferromagnetic interaction of J_{teo} = −0.85 cm^{-1}, validating both the magnitude and the antiferromagnetic nature of the fitted interaction.

For compound **6**, the fitting of the dc magnetic data was done by means of the Hamiltonian of eqn (2):

$$\begin{aligned}\hat{H} = {} & D[(\hat{S}_{zRe1})^2 + (\hat{S}_{zRe2})^2 - 5/2] + 2\beta H(g_{Re}\hat{S}_{Re} + g_{Gd}\hat{S}_{Gd}) \\ & - 2J(\hat{S}_{Re1}\hat{S}_{Re2})\end{aligned} \quad (2)$$

where the first term corresponds to the ZFS contribution of the Re^{IV} ions, while the second one accounts for the Zeeman effects of the two types of metal ions. A third term is included in eqn (2), assuming a non-negligible magnetic interaction between two rhenium(IV) monomers of different neighbouring chains. To avoid overparameterisation, we assume an isotropic g parameter for the rhenium(IV) ion and a fixed one for the gadolinium(III) ion [g_{Gd} = 2.0]. The values obtained from the best fit of the least-squares calculation are $|D_{Re}|$ = 10.9(6) cm^{-1}, g_{Re} = 1.88(1) and J = −0.51(2) K with R = 99.1%. As shown in Fig. 5, the calculated curve for **6** reproduces very well the experimental magnetic data in the whole temperature range. $|D_{Re}|$, g_{Re} and J values are in agreement with those determined for **1**. Nonetheless, the decrease in the $\chi_M T$ values might also respond to weak intramolecular interactions of the type $Gd^{III}\cdots Gd^{III}$ or, less probable, $Re^{IV}\cdots Gd^{III}$.[19]

To verify this last statement and confirm that these last interactions can be neglected in the fitting of the experimental data, we performed BS-DFT calculations (see the SI). For doing so, we used a cropped model containing two Gd^{III} and one Re^{IV} ions from one chain of the crystal structure (Fig. S5). The obtained J values were $J_1 = J_2 = J_3$ = 0.00 cm^{-1}, which supports the fact that there is no interaction between magnetic centres, at least at the calculation's precision level. A second run of calculations was performed on a simplified dinuclear $[ReBr_5(3,4\text{-pydc})]_2$ model in order to quantify the intermolecular magnetic exchange between Re^{IV} ions from both the same and neighbouring chains (Fig. S5). For this, we chose the rhenium-based metalloligands with the shortest intra- and interchain Br···Br distances, which are 4.716(1) and 4.421(1) Å, respectively.

In this case, the results were J_1 = 0.02 cm^{-1} (intramolecular) and J_2 = −0.57 cm^{-1} (intermolecular). These results are in agreement with the fitting of the experimental data, given that the predominant interaction would be a very weak antiferromagnetic coupling between adjacent chains, which might explain the below-expected decrease of $\chi_M T$ values at lower temperatures in the experimental curve. The weaker theoretically calculated exchange interaction in **6** compared to **1** correlates with its longer Br···Br distance, consistent with the expected trend for halogen···halogen magnetic interactions. However, this specific trend is not reflected in the experimentally derived J values for both compounds (Table 1).

Furthermore, CASSCF calculations were performed on CM1 (see the SI), for which values of g_{teo} = 1.80 and D_{teo} = 11.98 cm^{-1} were obtained. These values are in accordance with those found from the experimental data fitting for **6**, and also with those obtained both experimentally and theoretically for **1**.

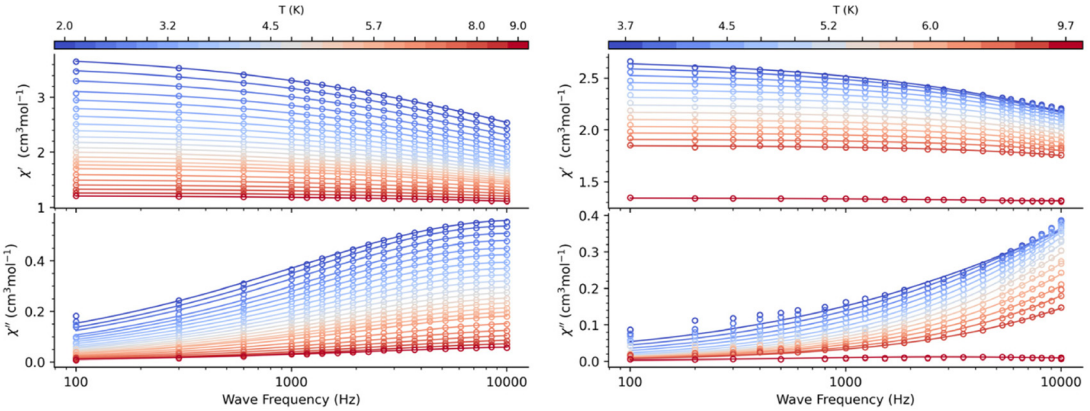

Fig. 6 Frequency dependence of χ'_M and χ''_M signals for **2** (left) and **4** (right) under an external dc magnetic field of 2000 G. Solid lines account for the theoretical generalised Debye fitting of the experimental data.

Table 1 Comparison between experimental and theoretical magnetic parameters for compounds **1** and **6**

	Experimental			Theoretical		
	g_{Re}	$\|D_{Re}\|^a$	J^a	g_{Re}	$D_{Re}{}^a$	J^a
1	1.89(1)	7.39(4)	−0.22(1)	1.79	7.08	−0.85
6	1.88(1)	10.9(6)	−0.51(2)	1.80	11.98	−0.57 [b]

[a] In cm^{-1}. [b] Corresponding to the shortest interchain distance.

Despite some minor discrepancies, the remarkable agreement between experimental and theoretical approaches validates the proposed magnetic dinuclear models for the experimental data fitting and highlights the reliability of the methodologies employed.

Ac magnetic susceptibility. Alternating current (ac) magnetic susceptibility measurements were performed on microcrystalline samples of all the complexes. No out-of-phase ac signals (χ''_M) are observed at H_{dc} = 0 G. However, out-of-phase ac signals appear at low temperatures in **2** and **4**, with observable χ''_M maxima in **4**, when an external dc magnetic field (H_{dc} = 1000 and 2000 G) is applied (Fig. 7, S2 and S3). Thus, an ac characterisation of **2** and **4** has been performed in the temperature range of 2–10 K and under a 3.5 G ac field oscillating at different frequencies. These magnetic features would indicate that **2** and **4** exhibit a field-induced slow relaxation of the magnetisation phenomenon, which could be assignable to a single-ion magnet (SIM) behaviour.[41] Nevertheless, the relaxation dynamics of the two complexes is not equally affected by the external dc magnetic fields. While the H_{dc} = 2000 G seems to be already optimal for compound **4** (with the presence of more χ''_M maxima that shift towards higher frequencies), this magnetic field is less useful for studying the magnetic relaxation in **2**, where no χ''_M maxima in the χ''_M *versus T* plot occurs (Fig. S2 and S3). While no significant dependence of χ''_M with the external field is observed in **2**, the χ''_M peaks appear at higher temperatures with increasing H in **4**.

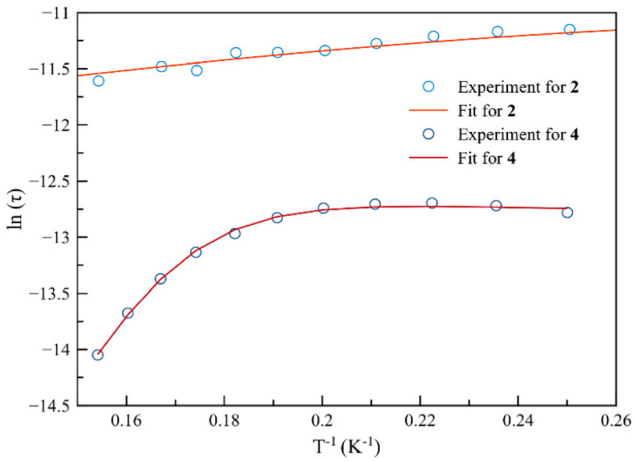

Fig. 7 Ln(τ) *vs. T* plot for **2** and **4** under an external dc magnetic field of 2000 G. Solid red and orange lines account for the theoretical fitting of the data, composed of the sum of RTB and Orbach relaxation models. Best-fit parameters are summarized in Table 2.

Table 2 Best-fit parameters obtained for the variation of the relaxation times with temperature for **2** and **4**

	U_{eff}/K	τ_o/s	F/K^k s	K
2	6.5(2)	$5(3) \times 10^{-5}$	1.9×10^5	1.55(76)
4	82(4)	$2.9(2) \times 10^{-11}$	4.7×10^5	0.23(20)

As shown in Fig. 6, maxima in the χ''_M *vs.* frequency (Hz) plot are not observed in **2** or in **4**. Nevertheless, it has been possible to fit the experimental data collected under a dc field of 2000 G by means of the CC-FIT 2 software by using a generalised Debye model.[42] The relaxation times (τ) were obtained for each frequency and revealed an unusual trend at low temperatures, in which they decrease with decreasing temperatures. This phenomenon, known as the Reciprocating Thermal Behaviour (RTB), has been previously fitted *via* the phenomenological equation $\tau_{RTB}{}^{-1} = FT^{-k}$ with $k > 0$.[43] The experimental

ac data were fitted as shown in Fig. 6 through two mechanisms for spin–lattice relaxation of the magnetisation, namely RTB (FT^{-k}) and Orbach [$\tau_o^{-1}\exp(-U_{eff}/k_BT)$], where τ_o is the pre-exponential factor, τ is the relaxation time, U_{eff} is the barrier to relaxation of the magnetisation and k_B is the Boltzmann constant. The best least-squares fit of the experimental data was obtained through eqn (3):

$$\tau^{-1} = {\tau_{RTB}}^{-1} + {\tau_{Orbach}}^{-1}. \quad (3)$$

The calculated parameters are U_{eff} = 6.5(2) K, τ_o = 2.5(3) × 10^{-5} s, $F = 1.9 \times 10^5$ K^k s^{-1} and k = 1.5(5) for compound **2** and U_{eff} = 82(4) K, τ_o = 2.9(2) × 10^{-11} s, $F = 4.7 \times 10^5$ K^k s^{-1} and k = 0.23(20) for compound **4**.

From these results, it is worth noting that the U_{eff} and τ_o values obtained for compound **2** are among what has been previously reported for this type of complexes showing SIM or SMM behaviours.[17,41,44] However, the U_{eff} value obtained for compound **4** is relatively higher than those previously reported for octacoordinate Dy^{III}-based polynuclear complexes exhibiting a squared-antiprismatic coordination geometry.[45,46] Nevertheless, the fitted τ_o value in **4** is in the range of the usually reported for similar Dy^{III}-based compounds (10^{-5}–10^{-11} s).[47,48] The addition of the reciprocating thermal behaviour term to the equation visually improved the fit, though a detailed analysis of the resulting parameters is not considered, as they have only phenomenological meaning.

In light of the analysis of the dc data for the analogous compound **6**, and the results obtained by the analysis of the ac experiments, **2** and **4** might be considered as compounds that behave as chains of SIMs, with this property arising from the electronic structure of each independent Dy^{III} ion. Rhenium(IV) ions have not been considered the origin of the slow relaxation of magnetisation based on two key observations. First, previously reported rhenium(IV) compounds with pseudo-C_{4v} symmetry and Br···Br intermolecular interactions do not exhibit SIM behaviour.[22] Second, given that compounds **4–6** are isostructural, any significant ac signal intrinsic to the Re(IV) ion would also be observed in the Gd(III) and Tb(III) compounds. The absence of such signals in these derivatives confirms that the Re(IV) monomer is not the source of the slow relaxation of magnetisation. According to the previous comments, SCM behaviour in **2** and **4** would be discarded given the long Ln···Ln distances and the absence of any evidence of significant intramolecular magnetic exchange in these $Re^{IV}Dy^{III}$-based compounds.[17]

Conclusions

In summary, one Re^{IV}-based mononuclear complex (**1**) and five novel one-dimensional Re^{IV}–Ln^{III} [Ln^{III} = Dy(**2**/**4**), Tb(**3**/**5**), Gd (**6**)] complexes were synthesised using derivatives of the pyridinedicarboxylic acid as ligands. Compounds **1–6** were characterised structurally and magnetically. The resulting structural architecture depends strongly on the ligand geometry and the coordinating solvent that was used.

From this family of Re^{IV}–Ln^{III} systems, the Re^{IV}–Dy^{III} complexes (**2** and **4**) exhibit slow magnetic relaxation when an external dc field is applied, which is consistent with the single-ion magnet (SIM) behaviour, and the obtained U_{eff} values vary from 14.6 to 92.0 K. A phenomenological unusual relaxation mechanism, not fully understood by the community to date, needed to be considered to fit the relaxation times at low temperatures. The presence of short Br···Br halogen interactions—of both intra- and intermolecular type—appears to influence the low-temperature magnetic properties, particularly in the case of the mononuclear (**1**) and neutral-chain systems (**4–6**).

DFT and NEVPT2 calculations were performed to aid the interpretation of the magnetic parameters derived from the experimental fitting. These results highlight the versatility of systems based on highly anisotropic 5d (Re^{IV}) and 4f (Ln^{III}) metal ions for constructing magnetically functional molecule-based materials, which could be suitable systems to be further studied in future information storage and molecular spintronics applications.

Author contributions

F. L., J. C., J. M.-L., C. R.-D. and R. G. conceived the idea and obtained funding for the project; C. R.-D. and R. G. designed the experiments; C. F.-A., C. R.-D., S. V. and A. L. synthesized and characterised the complexes; C. F.-A, C. R.-D., N. M., and L. S. carried out the crystallographic study; F. L., J. C., J. M.-L., S. V., R. C., and N. M. performed the magnetic study and the theoretical calculations; and C. R.-D., S. V., F. L., J. M.-L. and R. G. wrote and/or reviewed the manuscript. All authors have read and agreed to the published version of the manuscript.

Conflicts of interest

There are no conflicts to declare.

Data availability

The data of this investigation are available from the corresponding authors on reasonable request.

Supplementary information (SI) is available. Further crystallographic, magnetic and theoretical details are available in the SI. See DOI: https://doi.org/10.1039/d5dt01890k.

CCDC 2407409–2407414 contain the supplementary crystallographic data for this paper.[49a–f]

Acknowledgements

Financial support from the Comisión Sectorial de Investigación Científica (Uruguay, Project 453), Agencia Nacional de Investigación e Innovación (ANII, Uruguay, FCE_1_2021_1_167507) and PEDECIBA is gratefully

acknowledged. C. F. thanks ANII and S. V. thanks Comisión Académica de Posgrado (Universidad de la República) for scholarships. Funding supported by the Spanish MINECO (PID2019-109735GB-I00 and CEX2019-000919-M) and the Generalitat Valenciana (AICO/2020/183 and AICO/2021/295) is also acknowledged.

References

1 L. Bogani and W. Wernsdorfer, *Nat. Mater.*, 2008, **7**, 179–186.
2 T. Komeda, H. Isshiki, J. Liu, Y.-F. Zhang, N. Lorente, K. Katoh, B. K. Breedlove and M. Yamashita, *Nat. Commun.*, 2011, **2**, 217.
3 J. M. Clemente-Juan, E. Coronado and A. Gaita-Ariño, *Chem. Soc. Rev.*, 2012, **41**, 7464–7478.
4 J. Ferrando-Soria, J. Vallejo, M. Castellano, J. Martínez-Lillo, E. Pardo, J. Cano, I. Castro, F. Lloret, R. Ruiz-García and M. Julve, *Coord. Chem. Rev.*, 2017, **339**, 17–103.
5 E. Moreno-Pineda and W. Wernsdorfer, *Nat. Rev. Phys.*, 2021, **3**(9), 645–659.
6 M. Savadkoohi, D. Gopman, P. Suh, C. Rojas-Dotti, J. Martínez-Lillo and P. Tyagi, *ACS Appl. Electron. Mater.*, 2023, **5**, 3333–3339.
7 B. R. Sankhi, E. Peigney, H. Brown, P. Suh, C. Rojas-Dotti, J. Martínez-Lillo and P. Tyagi, *J. Magn. Magn. Mater.*, 2024, **611**, 172608.
8 A. Zabala-Lekuona, J. M. Seco and E. Colacio, *Coord. Chem. Rev.*, 2021, **441**, 213984.
9 R. Sessoli, M. E. Boulon, A. Caneschi, M. Mannini, L. Poggini, F. Wilhelm and A. Rogalev, *Nat. Phys.*, 2015, **11**(1), 69–74.
10 C. A. Goodwin, F. Ortu, D. Reta, N. F. Chilton and D. P. Mills, *Nature*, 2017, **548**, 439–442.
11 A. C. Aragonès, D. Aravena, J. I. Cerdá, Z. Acís-Castillo, H. Li, J. A. Real, F. Sanz, J. Hihath, E. Ruiz and I. Díez-Pérez, *Nano Lett.*, 2016, **16**(1), 218–226.
12 R. Rabelo, L. Toma, N. Moliner, M. Julve, F. Lloret, J. Pasán, C. Ruiz-Pérez, R. Ruiz-García and J. Cano, *Chem. Commun.*, 2020, **56**, 12242–12245.
13 K. S. Pedersen, A. Vindigni, R. Sessoli, C. Coulon and R. Clérac, *MMM: C&A*, 2017, 131–159.
14 F. Houard, G. Cucinotta, T. Guizouarn, Y. Suffren, G. Calvez, C. Daiguebonne and K. Bernot, *Mater. Horiz.*, 2023, **10**(2), 547–555.
15 N. Ishikawa, M. Sugita, T. Ishikawa, S. Koshihara and Y. Kaizu, *J. Am. Chem. Soc.*, 2003, **125**, 8694–8695.
16 J. P. Costes, L. Vendier and W. Wernsdorfer, *Dalton Trans.*, 2010, **39**, 4886–4892.
17 M. Orts-Arroyo, I. Castro, F. Lloret and J. Martínez-Lillo, *Dalton Trans.*, 2020, **49**, 9155–9163.
18 X.-Y. Wang, C. Avendaño and K. R. Dunbar, *Chem. Soc. Rev.*, 2011, **40**, 3213–3238.
19 J. Martínez-Lillo, L. Cañadillas-Delgado, J. Cano, F. Lloret, M. Julve and J. Faus, *Chem. Commun.*, 2012, **48**, 9242–9244.
20 C. Pejo, G. P. Guedes, M. A. Novak, N. L. Speziali, R. Chiozzone, M. Julve, F. Lloret, M. G. F. Vaz and R. González, *Chem.-Eur. J.*, 2015, **21**, 8696–8700.
21 R. Chiozzone, R. González, C. Kremer, G. De Munno, J. Cano, F. Lloret, M. Julve and J. Faus, *Inorg. Chem.*, 1999, **38**, 4745–4752.
22 J. Martínez-Lillo, J. Faus, F. Lloret and M. Julve, *Coord. Chem. Rev.*, 2015, **289–290**, 215–237.
23 S. K. Singh and G. Rajaraman, *Nat. Commun.*, 2016, **7**, 10669.
24 L. Arizaga, W. Cañon-Mancisidor, J. S. Gancheff, R. A. Burrow, D. Armentano, F. Lloret, R. González, C. Kremer and R. Chiozzone, *Polyhedron*, 2019, **174**, 114165.
25 *Inorganic Synthesis*, ed. J. Kleinberg, McGraw-Hill, New York, 1963, vol. 7, p. 190.
26 G. A. Bain and J. F. Berry, *J. Chem. Educ.*, 2008, **85**, 532–536.
27 G. M. Sheldrick, *SHELXL-2018. Program for Crystal Structure Refinement*, University of Göttingen, Göttingen, 2018.
28 F. Neese, *WIREs Comput. Mol. Sci.*, 2022, **12**, e1606.
29 F. Weigend and R. Ahlrichs, *Phys. Chem. Chem. Phys.*, 2005, **7**, 3297–3305.
30 C. Angeli, R. Cimiraglia, S. Evangelisti, T. Leininger and J.-P. Malrieu, *J. Chem. Phys.*, 2001, **114**, 10252–10264.
31 R. Chiozzone, R. González, C. Kremer, M. F. Cerdá, D. Armentano, G. De Munno, J. Martínez-Lillo and J. Faus, *Dalton Trans.*, 2007, 653–660.
32 J. Martínez-Lillo, T. F. Mastropietro, G. De Munno, F. Lloret, M. Julve and J. Faus, *Inorg. Chem.*, 2011, **50**, 5731–5739.
33 Ch. H. Woodall, G. A. Craig, A. Prescimone, M. Misek, J. Cano, J. Faus, M. R. Probert, S. Parsons, S. Moggach, J. Martínez-Lillo, M. Murrie, K. V. Kamenev and E. K. Brechin, *Nat. Comm.*, 2016, **7**, 13870.
34 C. Rojas-Dotti, N. Moliner, R. González and J. Martínez-Lillo, *J. Coord. Chem.*, 2018, **71**, 737–747.
35 C. Rojas-Dotti, A. Sanchis-Perucho, M. Orts-Arroyo, F. Lloret and J. Martínez-Lillo, *C. R. Chim.*, 2019, **22**, 490–497.
36 M. Orts-Arroyo, A. Sanchis-Perucho, N. Moliner, I. Castro, F. Lloret and J. Martínez-Lillo, *Inorganics*, 2022, **10**, 32.
37 N. F. Chilton, R. P. Anderson, L. D. Turner, A. Soncini and K. S. Murray, *J. Comput. Chem.*, 2022, **34**, 1164–1175.
38 J. Martínez-Lillo, D. Armentano, G. De Munno, F. Lloret, M. Julve and J. Faus, *Inorg. Chim. Acta*, 2006, **359**, 3291–3296.
39 J. Martínez-Lillo, D. Armentano, N. Marino, L. Arizaga, R. Chiozzone, R. González, C. Kremer, J. Cano and J. Faus, *Dalton Trans.*, 2008, 4585–4594.
40 J.-L. Liu, K. S. Pedersen, S. M. Greer, I. Oyarzabal, A. Mondal, S. Hill, F. Wilhelm, A. Rogalev, A. Tressaud, E. Durand, J. R. Long and R. Clérac, *Angew. Chem., Int. Ed.*, 2020, **59**, 10306.
41 J. Martínez-Lillo, T. F. Mastropietro, E. Lhotel, C. Paulsen, J. Cano, G. De Munno, J. Faus, F. Lloret, M. Julve,

S. Nellutla and J. Krzystek, *J. Am. Chem. Soc.*, 2013, **135**, 13737–13748.
42 W. J. A. Blackmore, G. K. Gransbury, P. Evans, J. G. C. Kragskow, D. P. Mills and N. F. Chilton, *Phys. Chem. Chem. Phys.*, 2023, **25**, 16735–16744.
43 C. Rajnák and R. Boča, *Coord. Chem. Rev.*, 2021, **436**, 213808.
44 A. B. Ruiz-Muelle, A. García-García, A. A. García-Valdivia, I. Oyarzabal, J. Cepeda, J. M. Seco, E. Colacio, A. Rodríguez-Diéguez and I. Fernández, *Dalton Trans.*, 2018, **47**, 12783–12794.
45 J. J. Baldoví, E. Coronado, A. Gaita-Ariño, C. Gamer, M. Giménez-Marqués and G. Minguez-Espallargas, *Chem.-Eur. J.*, 2014, **20**, 10695–10702.
46 D. N. Bazhin, Y. S. Kudyakova, A. S. Bogomyakov, P. A. Slepukhin, G. A. Kim, Y. V. Burgart and V. I. Saloutin, *Inorg. Chem. Front.*, 2019, **6**, 40–49.
47 Y. Dong, P. Yan, X. Zou, T. Liu and G. Li, *J. Mater. Chem., C*, 2015, **3**, 4407–4415.
48 S. Biswas, S. Das, J. Acharya, V. Kumar, J. van Leusen, P. Kögerler, J. M. Herrera, E. Colacio and V. Chandrasekhar, *Chem.-Eur. J.*, 2017, **23**, 5154–5170.
49 (*a*) CCDC 2407409: Experimental Crystal Structure Determination, 2025, DOI: 10.5517/ccdc.csd.cc2lt3cx; (*b*) CCDC 2407410: Experimental Crystal Structure Determination, 2025, DOI: 10.5517/ccdc.csd.cc2lt3dy; (*c*) CCDC 2407411: Experimental Crystal Structure Determination, 2025, DOI: 10.5517/ccdc.csd.cc2lt3fz; (*d*) CCDC 2407412: Experimental Crystal Structure Determination, 2025, DOI: 10.5517/ccdc.csd.cc2lt3g0; (*e*) CCDC 2407413: Experimental Crystal Structure Determination, 2025, DOI: 10.5517/ccdc.csd.cc2lt3h1; (*f*) CCDC 2407414: Experimental Crystal Structure Determination, 2025, DOI: 10.5517/ccdc.csd.cc2lt3j2.